energies

MDPI

Article

Comprehensive Evaluation of Retrogression-Resistant Well Cement Systems Set at Different Temperatures and Cured at 200 °C

Jianwei Yu [1], Guodong Cheng [2], Jiankun Qin [3], Ziya Liao [1], Xueyu Pang [1,4,*], Jiapei Du [5], Kaihe Lv [1,4] and Jinsheng Sun [1,4,*]

[1] School of Petroleum Engineering, China University of Petroleum (East China), Qingdao 266580, China; b25020063@s.upc.edu.cn (J.Y.); 2317020209@s.upc.edu.cn (Z.L.); lkh54321@126.com (K.L.)
[2] SINOPEC Research Institute of Petroleum Engineering Co., Ltd., Beijing 102206, China; ggddcheng@sina.com
[3] Petroleum Engineering Technology Research Institute of Shengli Oilfield, SINOPEC, Dongying 257000, China; qinjiankun.slyt@sinopec.com
[4] State Key Laboratory of Deep Oil and Gas, China University of Petroleum (East China), Qingdao 266580, China
[5] School of Engineering, Royal Melbourne Institute of Technology, Melbourne, VIC 3001, Australia; jiapei.du@rmit.edu.au
* Correspondence: x.pang@upc.edu.cn (X.P.); sunjsdri@cnpc.com.cn (J.S.)

Abstract

Traditional silica-enriched oil well cement suffers from strength retrogression at high temperatures, hindering deep geoenergy resource development. This study comprehensively evaluates novel retrogression-resistant cement systems formulated with Portland cement, silica sand, fly ash, and ground blast furnace slag. Slurries with densities of 1.9–1.6 g/cm^3 were prepared by adjusting water content or adding hollow glass microspheres, and cured at 200 °C after initial setting at either 80 °C or 200 °C to simulate different field conditions. Results show that systems directly set at 200 °C maintained stable mechanical properties over 30 days, while those set at 80 °C exhibited significant strength gains. Permeability and pore structure remained stable or refined in all systems. Microscopic analyses (MIP, QXRD, TGA) reveal that low-temperature-set systems contain higher tobermorite and lower xonotlite and hydrogrossular contents, explaining their superior performance. Density reduction by water addition weakened properties, whereas hollow glass microspheres effectively preserved microstructure and strength. The C-(A)-S-H content remained stable throughout curing, and tobermorite increased over time, constituting the primary anti-retrogression mechanism. These findings provide insights into the roles of setting temperature and density regulation, supporting the design of durable cement systems for deep and ultra-deep wells.

Keywords: strength retrogression; setting temperature; fly ash; ground blast furnace slag; hollow glass microspheres

Check for updates

Academic Editor: Hossein Hamidi

Received: 7 September 2026
Revised: 12 October 2026
Accepted: 17 October 2026
Published: 25 October 2026

Copyright: © 2026 by the authors. Licensee MDPI, Basel, Switzerland. This article is an open access article distributed under the terms and conditions of the Creative Commons Attribution (CC BY) license.

1. Introduction

Portland cement is the primary sealant used during the completion of oil, gas, and geothermal wells to seal the annular space between the casing and the formation. Its long-term performance stability directly affects wellbore integrity, production safety, and the economic efficiency of these wells [1]. With the gradual depletion of shallow geoenergy resources, exploration and development activities are accelerating their shift toward deep

and ultra-deep reservoirs characterized by high-temperature and high-pressure (HPHT) environments [2]. In the development of deep oil, natural gas, and geothermal resources, the bottom hole static temperature (BHST) can exceed 200 °C, while the formation pressure may readily exceed 100 MPa or even 150 MPa [3–5]. Under such conditions, the hydration products and microstructure of well cement can change significantly during long-term curing [6]. Studies in recent years have revealed that curing temperature has a more adverse effect on the physical and mechanical performance of well cement than curing pressure [3,5]. According to previous studies, when curing temperature exceeds approximately 110 °C, the amorphous calcium silicate hydrate (C-S-H) gel in neat Portland cement tends to transform into high-calcium crystalline phases, leading to strength retrogression [1]. This phase transformation is usually accompanied by microstructure coarsening, increased permeability, and reduced compressive strength, making strength retrogression a major threat to long-term wellbore sealing integrity [1].

The strength stability of well cement under high-temperature conditions is affected by several factors, including setting temperature, curing temperature, curing time, slurry density, and cementitious composition. Among these factors, the influence of setting temperature has been gaining more and more attention in recent years. During the construction of geoenergy wells, the well cement may be subjected to high-temperature conditions in two different scenarios: (1) at the bottom-hole condition of deep and ultra-deep wells, the cement slurry is directly exposed to HPHT conditions before it sets (i.e., transforms from a fluid state into a hardened solid); (2) at the upper sections of deep wells or in steam injection wells, the cement slurry first sets to a solid state at relatively low temperatures before it is exposed to high temperatures at later stages [3,7–10]. To simulate the first scenario, the cement slurry should be placed in high-temperature-resistant curing molds and directly placed in HPHT curing autoclaves; the slurry also needs to be sufficiently retarded so that it does not set before reaching the final curing temperature. For the second scenario, the cement samples may be first cured in a water bath and demolded before they are placed in HPHT curing autoclaves for further curing. According to recent studies, well cement systems that are directly set and cured under HPHT conditions (simulating scenario 1) generally exhibit more severe strength retrogression than those that are initially set at low temperature before being exposed to high-temperature curing (simulating scenario 2) [11–16]. Therefore, setting temperature is a key factor that must be carefully considered in the design and evaluation of cement slurries.

For decades, adding silica flour or silica sand has been the most widely used approach to mitigate strength retrogression [9,17,18]. The addition of silica reduces the Ca/Si ratio of the cement system and promotes the formation of relatively more stable calcium silicate hydrate phases, such as tobermorite and xonotlite [9,17]. However, recent studies have shown that silica-enriched oil well cement systems still contain a significant amount of amorphous C-S-H as the main hydration products at 200 °C, and may experience severe long-term strength decline when they are directly set and cured under HPHT conditions [3]. This phenomenon can be primarily attributed to the poor stability of amorphous C-S-H at high temperatures, which induces gradual microstructure coarsening and strength retrogression [3]. To improve the long-term stability of well cement, different technical routes have been explored, including optimization of silica dosage and particle size, partial replacement of crystalline silica with silica fume, incorporation of nanomaterials, and addition of aluminum-bearing supplementary cementitious materials [3,19]. In particular, the combined use of silica sand with reactive alumina sources, such as fly ash and granulated blast furnace slag (GBFS), has shown strong potential for developing anti-strength-retrogression cement systems [19]. The incorporation of alumina into hydration products can transform the amorphous C-S-H phase to the more stable amorphous C-A-S-H phase, inhibit the

formation of unfavorable crystalline phases such as xonotlite, and thereby maintain a refined pore structure and stabilize the mechanical properties of set cement during long-term high-temperature curing [19–21].

Despite these advances, the performance of newly developed anti-strength-retrogression well cement systems has not been fully understood. Existing studies have mainly focused on the effectiveness of specific admixture combinations under limited curing conditions, while the influences of slurry density, setting temperature, and curing temperature on the long-term strength stability of these systems remain unclear. This limitation is important for field applications because low-density cement slurries are often required in fractured, low-pressure, or leakage-prone formations [22–24], where conventional high-density slurries may induce or aggravate lost circulation [25–27]. Low-density cement systems feature low solid content, high initial porosity, and more significant strength retrogression under high temperature and high pressures [19]; thus, the strength retrogression of low-density slurry under different setting temperatures needs to be further investigated. Hollow glass microspheres (HGMs) are widely used by the industry to optimize the performance of low-density well cement systems [28–30]; however, it is not yet clear whether this approach is effective in retrogression-resistant well cement systems at high temperatures.

This study aims to systematically investigate the effects of slurry density and initial setting temperature on the long-term performance of anti-strength-retrogression cement systems. Retrogression-resistant cement systems with different densities were prepared and subjected to different initial setting temperatures before long-term curing at 200 °C. The evolution behaviors of compressive strength, water permeability, pore structure, and phase composition were evaluated to clarify the relationships among slurry density, setting temperature, hydration product evolution, and mechanical properties of well cement. Quantitative X-ray diffraction (QXRD) analysis combined with the partial or no known crystal structure (PONKCS) method and thermogravimetric analysis was used to analyze the phase evolution of the set cement. The results are expected to provide a better understanding of the long-term stability of anti-strength-retrogression cement systems and support the design of cement slurries for deep and ultra-deep well applications.

2. Materials and Methods

2.1. Materials

The Class G oil well cement used in this study was provided by Sichuan Jiahua Enterprise Co., Ltd. (Leshan, Sichuan, China). Various mineral admixtures were employed in this study to mitigate well cement strength retrogression at high temperatures, including fly ash (FA) produced by Shuozhou Power Plant in Shuozhou, Shanxi, China; silica sand with a median particle size of 53 μm supplied by Kuqa Drilling Materials Co. in Kuqa, Xinjiang, China; and granulated blast furnace slag (GBFS) supplied by Shandong Qingyun Kangjing Building Materials Co., Ltd. (Qingyun, Shandong, China). The physical properties of the cement and mineral admixtures were measured using a laser particle size analyzer (Mastersizer 2000, manufactured by Malvern Instruments Ltd., Great Malvern, UK) and a pycnometer (Model UltraPYC 1200e by Quantachrome Instrument, Boynton Beach, FL, USA), with the results presented in Figure 1 and Table 1. The oxide compositions of the cement and mineral admixtures were determined by X-ray fluorescence (XRF) spectrometry and are presented in Table 1. As shown in Table 1, the dominant oxides in FA are alumina and silica, while the dominant oxides in GBFS are calcium oxide and silica. The compositions of the cement and mineral admixtures were also evaluated by X-ray diffraction analysis, with the results presented in Figure 2 and Table 2. GBFS is almost entirely amorphous, with only trace amounts of crystalline phases, while fly ash contains 89.5% amorphous phases.

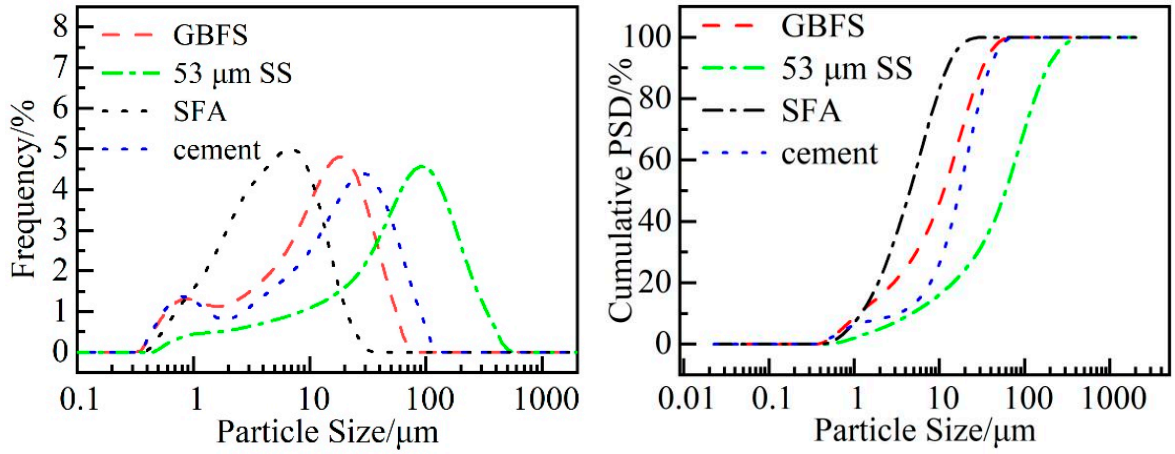


Figure 1. Particle size distribution of mineral admixtures: (**a**) Particle size distribution frequency; (**b**) cumulative particle size distribution.

Table 1. Characterization of Jiahua class G cement and mineral admixtures.

Parameters		Class G Cement	GBFS	53 μm Silica	FA
oxide/wt.%	Al_2O_3	3.44	14.00	1.03	39.29
	CaO	63.76	43.40	1.45	1.72
	Fe_2O_3	5.36	0.48	0.87	3.64
	K_2O	0.45	0.30	0.26	0.49
	TiO_2	—	0.84	—	1.90
	MgO	1.36	8.27	0.40	0.33
	Na_2O	0.49	0.48	0.19	0.07
	SO_3	3.22	3.42	0.21	1.68
	P_2O_5	3.44	0.02	0.02	0.15
	SiO_2	21.01	27.82	95.41	50.55
f-CaO	—	0.47	0.04	—	0.05
Loss on Ignition (LOI)	—	1.32	0.18	—	0.40
density/($g \cdot cm^{-3}$)	—	3.14	3.30	2.67	2.55
D_{10}/μm	—	—	1.12	4.04	1.20
D_{50}/μm	—	12.7	11.14	53.00	4.49
D_{90}/μm	—	—	31.80	163.00	12.23
Specific Surface Area (SSA)/($m^2 \cdot g^{-1}$)	—	520	423	234	805

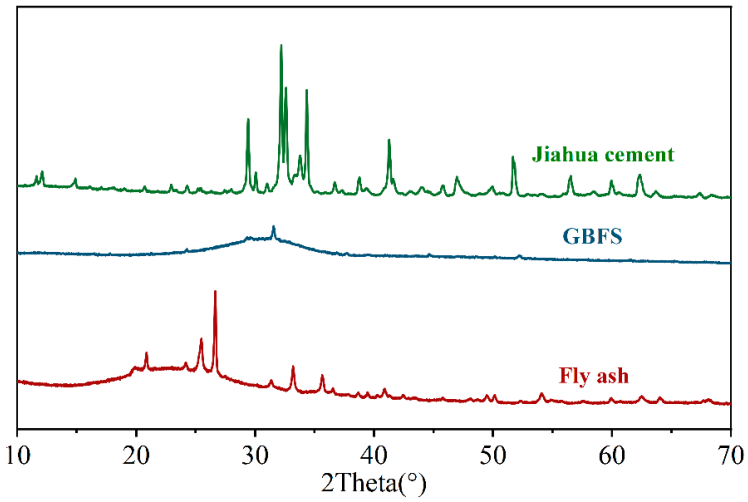


Figure 2. XRD profiles of Jiahua class G cement, GBFS and fly ash.

Table 2. QXRD main phase analysis results of Class G cement and fly ash.

Class G Cement		Fly Ash	
Phase	Mass %	Phase	Mass %
C_3S	49.88	Quartz	3.0
C_2S	26.40	Hematite	1.9
C_3A	2.96	Anhydrite	2.2
C_4AF	12.21	Muscovite 2M1	3.3
gypsum	3.27	Amorphous	89.5
hemihydrate	1.20	others	0.1
periclase	0.86	-	-
portlandite	0.02	-	-
others	2.98	-	-

High-temperature chemical admixtures, including a suspension aid, a dispersant, a retarder, a fluid-loss additive, and a defoamer, used to adjust the cement slurry properties were supplied by Tianjin CNPC Boxing Technology Co., Ltd. (Tianjin, China). The dispersant, retarder and fluid-loss additives used were all water suspensions with a solid activity of 20%. The high-temperature setting systems were optimized using these additives such that they have zero free fluid and good sedimentation stability. Thickening time tests of similar designs have been presented in our previous work, which demonstrated the operational feasibility of these slurries [31]. Diutan gum (DG), a suspension aid used to further improve the sedimentation stability of the cement slurry (especially in low-density slurries with high water-to-cement ratios), was provided by CP Kelco Biological Co., Ltd. (Rizhao, China). Hollow glass microspheres (HGM), with a density of 0.38 g/cm^3 and a crush pressure of 38 MPa, manufactured by Anhui Triumph Base Material Technology Co., Ltd. (Hefei, Anhui, China), were used to produce low-density slurries with high strength.

2.2. Design and Preparation of Cement Slurries

The cement slurry formulation designs are shown in Table 3, where all components are expressed in terms of by weight of cement (BWOC). It is worth noting that the porosity values in Table 3 are calculated solely for the purpose of relative comparison between different slurries during the formulation design period. All cement slurry formulations were designed with a CaO/SiO_2 molar ratio of approximately 0.83, using the chemical formula of tobermorite (a favorable high-temperature hydrate phase) as the reference. The dosages of additives in all slurries were optimized to achieve suitable pumpable time and workability. Systems N1–N4 were directly set and cured at high temperature (200 °C) to simulate cementing conditions in deep and ultra-deep wells. The design density of N1 was 1.90 g/cm^3. Based on N1, the densities of N2 and N3 were reduced by adding water, giving design densities of 1.75 and 1.60 g/cm^3, respectively. N4 was prepared by adding hollow glass microspheres to N1 to reduce the slurry density to 1.60 g/cm^3. Systems n1–n4 were initially set at a relatively low temperature of 80 °C and then subjected to high-temperature curing (200 °C) to simulate the cementing conditions of steam-injection wells and the upper sections of high-temperature wells. The solid components in n1–n4 were the same as those in N1–N4, with primary differences in chemical additives. The high-temperature retarder, suspension aid and fluid-loss additives were not used in the low-temperature setting slurries n1–n4. This is because excessive polymer additives can lead to super-retardation of the cement slurry at low temperatures. Although the kinetics of cement hydration induced by chemical additives may also influence the properties of the set cement, the effect is considered to be minimal, as the cement has reached 100% hydration after curing at 200 °C for 2 days.

Table 3. Cement slurry formulation design, density and calculated initial porosity (% BWOC).

Formula	N1	N2	N3	N4	n1	n2	n3	n4
Class G cement	100	100	100	100	100	100	100	100
FA	20	20	20	20	20	20	20	20
GBFS	80	80	80	80	80	80	80	80
53 μm silica sand	82	82	82	82	82	82	82	82
HGM	—	—	—	19.5	—	—	—	18
Suspension aid	2.5	5	7.5	2	—	—	—	—
Diutan gum	—	0.25	0.3	—	0.15	0.25	0.5	0.1
Retarder	7.5	7.5	7.5	7.5	—	—	—	—
Fluid loss additive	6.0	6.0	6.0	6.0	—	—	—	—
Dispersant	7.5	7.5	7.5	7.5	1.5	0.5	—	3.0
Defoamer	0.5	0.5	0.5	0.5	0.5	0.5	0.5	0.5
Water	95.9	139	204.3	95.9	111.7	153.8	217	111.7
Slurry density (g/cm^3)	1.9	1.75	1.6	1.6	1.9	1.75	1.6	1.6
Calculated initial porosity (%)	52.9	60.6	68.4	42.6	54.3	62	69.6	44.1

Note: The calculated initial porosity is the percentage of the total liquid volume in the cement slurry, including the added water and the water contained in liquid admixtures.

The cement slurries were prepared as follows: First, each slurry was premixed without fly ash according to the standard API procedure. Fly ash was then incorporated under low-speed stirring at 600 rpm. After all fly ash had been added, the slurry was further mixed at 3000 rpm for 35 s. At least six specimens were prepared for each formulation. Systems N1–N4 were directly set and cured under HPHT conditions (200 °C, 30 MPa) for 2 d. As the curing pressure is lower than the crush pressure of the HGM, the microspheres remain intact during HPHT curing. The autoclave was then cooled, and all specimens were demolded. Three specimens from each group were cut for testing, while the remaining three were returned to the HPHT autoclave for an additional 28 d of curing under the same conditions (200 °C, 30 MPa). For the low-temperature setting systems, compressive strength and permeability were also measured after 1 d of curing at 80 °C in order to evaluate their initial macroscopic properties before subsequent high-temperature curing.

2.3. Experimental and Analytical Methods

2.3.1. Macroscopic Property Tests

The macroscopic properties of the set cement were evaluated by compressive strength and water permeability tests. Compressive strength was measured using a UTM5105X computer-controlled electronic universal testing machine (Shenzhen SUNS Technology Stock Co., Ltd., Shenzhen, China) with a maximum load capacity of 150 kN. Water permeability was measured using an apparatus manufactured by Haian Huacheng Co. (Nantong, China) according to the Chinese National Standard GB/T 19139-2012. The inlet pressure was 2 MPa, the outlet pressure was atmospheric pressure, and the confining pressure was 5 MPa for the water permeability tests. This article uses μm^2 as the unit for permeability testing, and the conversion formula to mD is 1 μm^2 = 1.013 × 10^6 mD.

2.3.2. Microstructural Characterization

The microstructure of the set cement was characterized by mercury intrusion porosimetry (MIP). Cylindrical specimens were sliced into thin discs and then crushed into small fragments with a maximum size of less than 5 mm and a total mass of approximately 1 g. The fragments were weighed and placed in a penetrometer, and mercury was introduced into the low-pressure chamber under vacuum (0–0.2 MPa). The apparent density and porosity were determined from the change in weight of the penetrometer with and without the sample. The penetrometer was then transferred to the high-pressure station, where

the pressure was raised from atmospheric to 220 MPa and subsequently reduced back to atmospheric at the same rate. In calculating the pore size distribution, the surface tension of mercury was taken as 0.485 N/m and the contact angle between mercury and the hardened cement as 140°.

2.3.3. Phase Composition Analysis

The phase composition of the set cement was analyzed by thermogravimetric analysis (TGA) and X-ray diffraction (XRD). XRD data were collected using a benchtop X-ray diffractometer (Aeris, 600 W Cu anode source, λ = 1.541 Å; Panalytical, UK). The diffractometer operated at 40 kV and 15 mA. All scans were recorded over a 2θ range of 5–70° with a step size of 0.02°, and the total measurement time for each scan was approximately 30 min. Before XRD testing, the samples were vacuum-dried for 3 d and then ground into fine powder. TGA was performed using a Setline STA instrument (Setaram, France) under a nitrogen atmosphere. Sample preparation was similar to that used for XRD analysis. For each test, approximately 80 mg of powder was placed in an alumina crucible. The temperature was first increased to 100 °C at a heating rate of 10 °C/min and held for 1 h to remove residual evaporable water. The temperature was then increased from 100 °C to 1000 °C at the same heating rate to remove non-evaporable water. The cumulative weight loss over the entire heating process was taken as the total water content of the sample and was subsequently used for quantitative XRD analysis.

2.3.4. Phase Analysis by Rietveld Method and PONCKS Model

Rietveld-based quantitative X-ray diffraction (QXRD) analysis is designed for evaluating the phase composition of a material with known crystal structures. However, the compositions of both fly ash and GBFS are primarily amorphous phases with no ordered structures, and the hydrated cement also produces amorphous phases, such as C-(A)-S-H. During this study, the partial or no known crystal structures (PONKCS) method was employed to build pseudo-structure models for amorphous phases in fly ash and GBFS for the purpose of performing Rietveld analysis. In order to quantify the contents of amorphous hydration products, a single crystal silicon ground into fine powder was used as an external standard during the XRD tests. More details on the Rietveld refinement, including the construction and verification of the pseudo-structure models and the calculations involving the external standard method, can be found in our previously published work [19].

3. Results and Discussion

3.1. Compressive Strength Test Results and Analysis

Figure 3 shows the compressive strength test results of set cement with different densities, initially set at different temperatures (200 °C or 80 °C) and then cured at 200 °C for 2 d to 30 d. As shown in Figure 3, the systems directly set and cured at 200 °C maintained relatively stable strength from 2 d to 30 d. As expected, reducing slurry density by water addition significantly decreased the compressive strength of the set cement. Slurry N1, with a density of 1.90 g/cm^3, exhibited an average compressive strength of approximately 28 MPa, whereas slurry N3, with a density of 1.60 g/cm^3, showed an average compressive strength of only approximately 7.5 MPa, which was about 70% lower than that of N1 at the corresponding curing ages. In contrast, slurry N4, which had the same density as N3 but was prepared using hollow glass microspheres, had an average compressive strength of approximately 20 MPa. This value was much higher than that of N3, primarily because the use of hollow glass microspheres reduced the water/cement ratio and limited the formation of additional capillary pores. These results suggest that hollow glass microspheres can be

used to prepare high-performance low-density well cement slurries, even under ultra-high-temperature conditions.

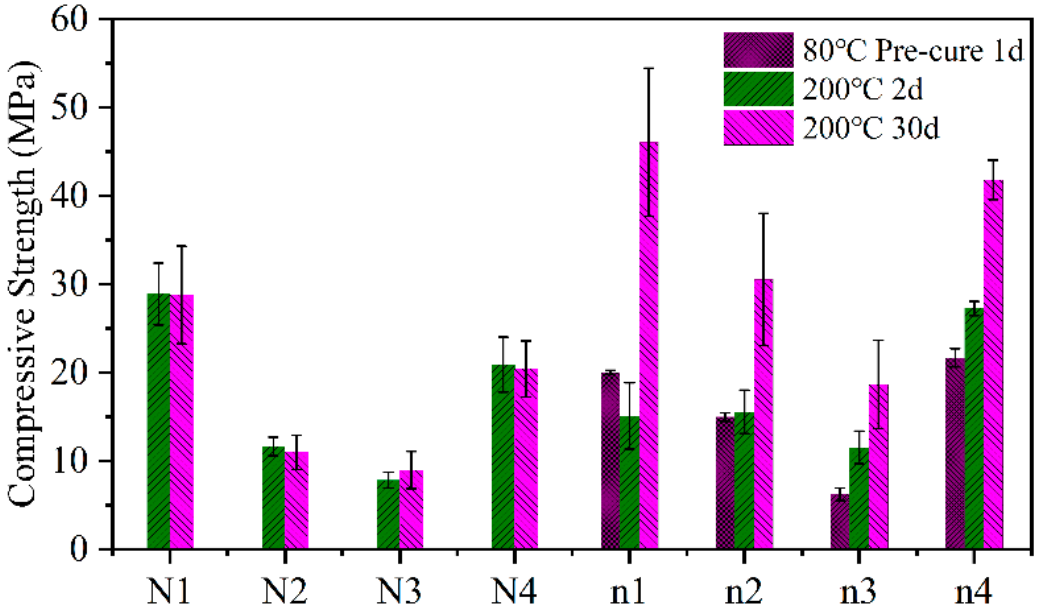


Figure 3. Compressive strength test results of set cement cured from 2 d to 30 d (N1–N4: set and cured at 200 °C; n1–n4: set at 80 °C for 1 d and then cured at 200 °C).

Figure 3 also shows that the strength of the slurry systems initially set at 80 °C increased from 2 d to 30 d. Initial setting at the relatively low temperature of 80 °C led to comparable 2 d strength (except for slurry n1) but significantly higher 30 d strength compared with the systems directly set and cured at 200 °C. For the low-density slurries (n2, n3, and n4), the 30 d strengths of the low-temperature-set systems were more than twice those of their high-temperature-set counterparts (N2, N3, and N4). The 30 d strength of n1 reached 45 MPa, which was approximately 60% higher than that of N1. In addition, the strengths of the systems set at 80 °C for 1 d were lower than those of the corresponding systems after 2 d of curing, indicating that continued curing at 200 °C further promoted early strength development.

3.2. Water Permeability Test Results and Analysis

Figure 4 shows the effects of setting temperature, curing time and slurry density on the permeability test results of different well cement systems. As shown in Figure 4, the permeability of set cement at both curing ages increased significantly with decreasing slurry density due to higher water content. However, the use of HGM to reduce slurry density (slurry N4) effectively mitigated the permeability increase. The permeability of the high-density system N1 increased by 2 times from 2 d to 30 d but remained at a very low level (~3×10^{-6} μm^2) after 30 d of curing. The permeability of all other high-temperature setting systems either remained stable or decreased with time. Figure 4 also shows that the permeability of the set cement cured at 80 °C for 1 d initially decreased with decreasing slurry density (from n1 to n2) before it increased sharply. This may be due to the fact that the higher water content in slurry n2 promoted a degree of hydration of the cement, which led to higher tortuosity of the pore structure. Upon high-temperature exposure for 2 d, the permeability of slurries n1, n2 and n4 increased significantly, possibly due to the crystalline transformation of amorphous hydration products. However, slurry n3, which has an extremely high initial permeability (2.9×10^{-4} μm^2), exhibited reductions in permeability upon high-temperature exposure. Therefore, the differences in set cement permeability

among slurries of different densities were relatively small in the low-temperature setting systems after 2 d of curing at 200 °C. Additionally, permeability of the low-temperature setting systems experienced much more significant reductions over long-term curing to 30 d. In particular, the permeability of slurry n4 containing HGM decreased to 6×10^{-7} μm^2, which is even much lower than that of the high-density slurries N1 and n1.

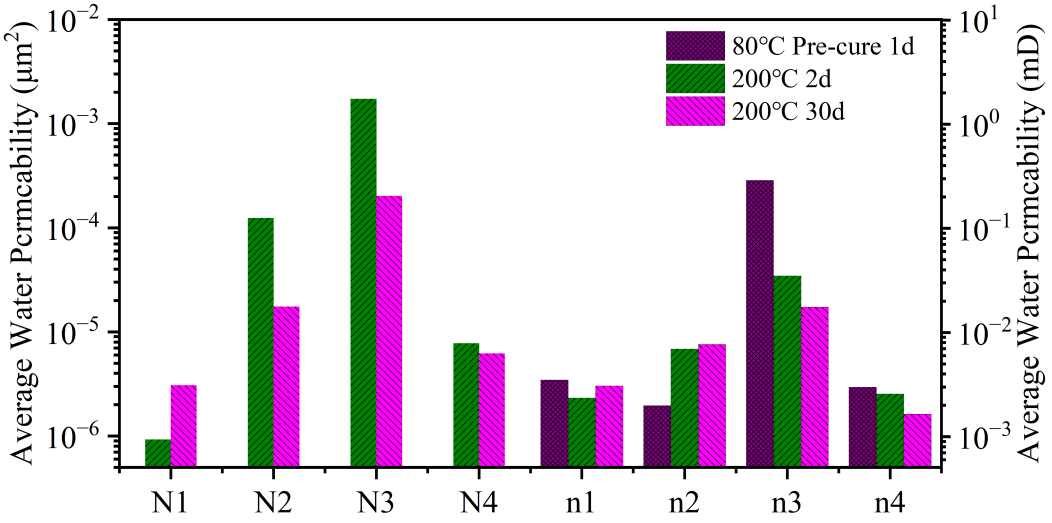


Figure 4. Water permeability test results of set cement cured from 2 d to 30 d (N1–N4: set and cured at 200 °C; n1–n4: set at 80 °C for 1 d and then cured at 200 °C).

3.3. Mercury Intrusion Porosimetry (MIP) Analysis

Figure 5 shows the MIP test results of the different cement slurry systems. Overall, all slurries exhibited highly stable pore structures over time, regardless of setting regime or slurry density. The total porosities of the set cement were lower than the calculated initial values listed in Table 3 due to the generation of hydration products. Slurry N2 showed a relatively noticeable increase in total porosity from 46.5% to 52.5%, whereas slurry N4 showed the opposite trend, with total porosity decreasing from 45.4% to 41.1%. The mode pore size, defined as the peak of the pore size distribution curve or the most frequently occurring pore diameter, decreased with increasing curing time for almost all samples, except for slurry n1, which showed only a slight increase. These results are consistent with the compressive strength and water permeability results and further demonstrate the effectiveness of the combined use of fly ash, slag, and silica sand as anti-strength-retrogression materials. With decreasing slurry density, both total porosity and pore size increased, explaining the lower strength and higher permeability of the low-density systems. Reducing density by adding hollow glass microspheres instead of additional water effectively mitigated increases in porosity and pore size, which explains why strength could remain relatively stable despite density reduction. According to previous studies [19], pores in cementitious materials can be classified as harmless pores (<20 nm), less harmful pores (20–50 nm), harmful pores (50–200 nm), and more harmful pores (>200 nm). Figure 6 shows the proportions of different pore types in the tested samples. Apparently, the total contents of harmful pores and more harmful pores in the low-temperature setting systems were significantly less than those in the high-temperature setting systems at all densities and curing ages. In almost all samples except n1, the combined proportion of harmful and more harmful pores decreased with increasing curing time. Compared with the samples set at high temperature, those set at low temperature had narrower pore size distributions and smaller mode pore sizes. For the HGM-bearing systems N4 and n4, the measured total porosity may be somewhat overestimated because part of the HGM can collapse during mercury intrusion (with an intrusion pressure of 220 MPa).

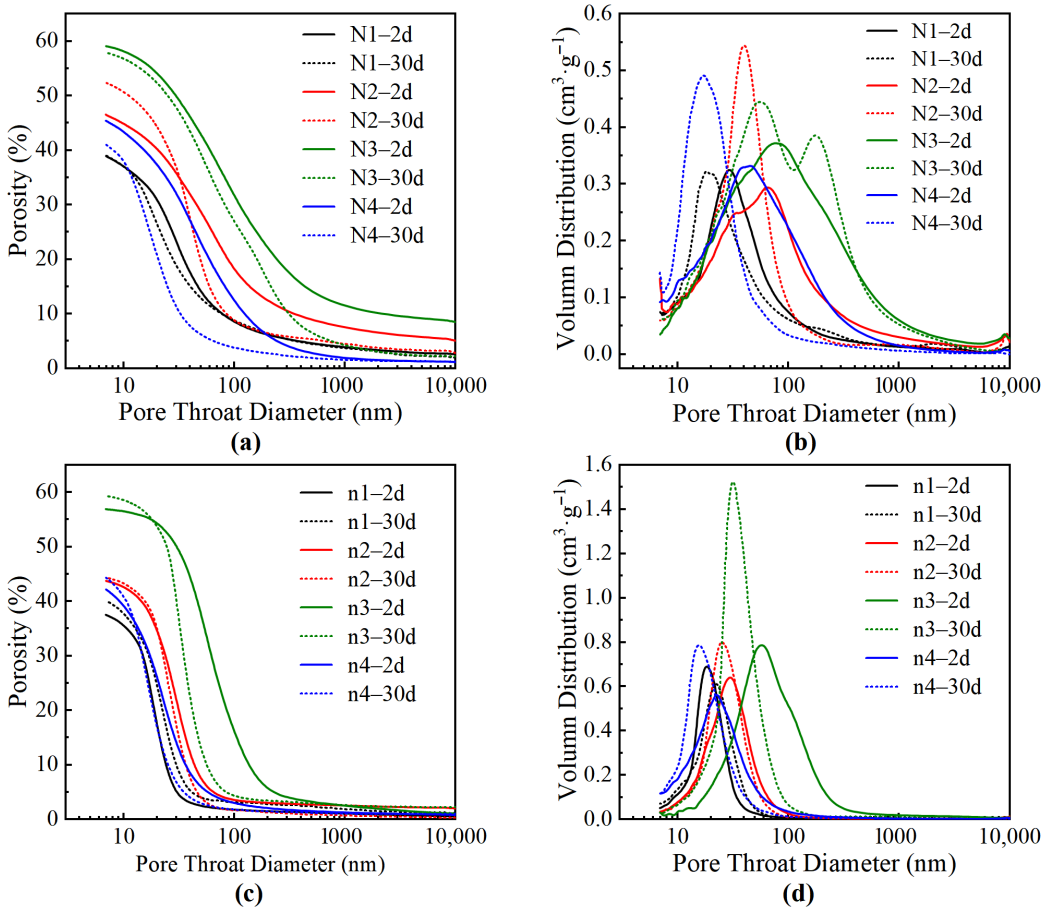


Figure 5. MIP test results of set cement during 2 d–30 d of curing: (**a**) Cumulative pore volume of high-temperature setting systems; (**b**) pore size distribution of high-temperature setting systems; (**c**) cumulative pore volume of low-temperature setting systems; (**d**) pore size distribution of low-temperature setting systems.

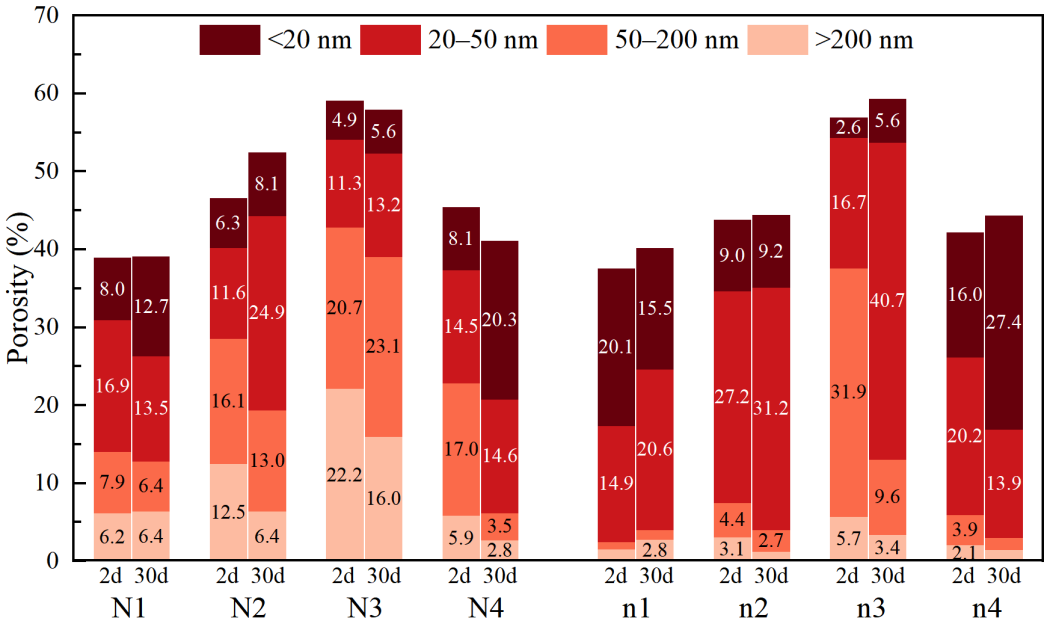


Figure 6. Pore size classification results of set cement during 2 d–30 d of curing. N1–N4: high-temperature setting systems; n1–n4: low-temperature setting systems.

In summary, the low-temperature setting systems developed a finer microstructure than the high-temperature setting systems, which is consistent with the compressive strength and water permeability results. The microstructure of the set cement coarsened significantly with increasing water-to-cement ratio (i.e., decreasing density). However, reducing density by incorporating hollow glass microspheres was beneficial for maintaining a refined pore structure. In most cases, the pore structure improved with curing time, which may explain why the water permeability of the low-density systems remained relatively stable over time or even decreased with time in certain cases.

3.4. X-Ray Diffraction (XRD) Analysis

Figure 7 summarizes the XRD test results of both the high-temperature setting systems and the low-temperature setting systems. The main hydration products included semi-crystalline C-(A)-S-H, tobermorite, xonotlite, and hydrogrossular. As shown in the figure, the crystallinity of both high- and low-temperature setting systems increased with curing time, as confirmed by slight sharpening of the broad peak in the 28.5–33.5° range and a minor increase in the overlapping peak at 28.9° assigned to tobermorite and xonotlite. For the high-temperature setting systems, the tobermorite peak became more intense, while the peaks at 24.5° and 25.5° corresponding to xonotlite weakened notably. Compared with the high-temperature setting systems, the low-temperature setting systems showed lower hydrogrossular intensity, as indicated by the weaker peak at 32.9°. Because hydrogrossular mainly crystallizes from semi-crystalline C-(A)-S-H within the 28.5–33.5° range, the lower hydrogrossular content suggests that C-(A)-S-H remained more stable in the low-temperature setting systems.

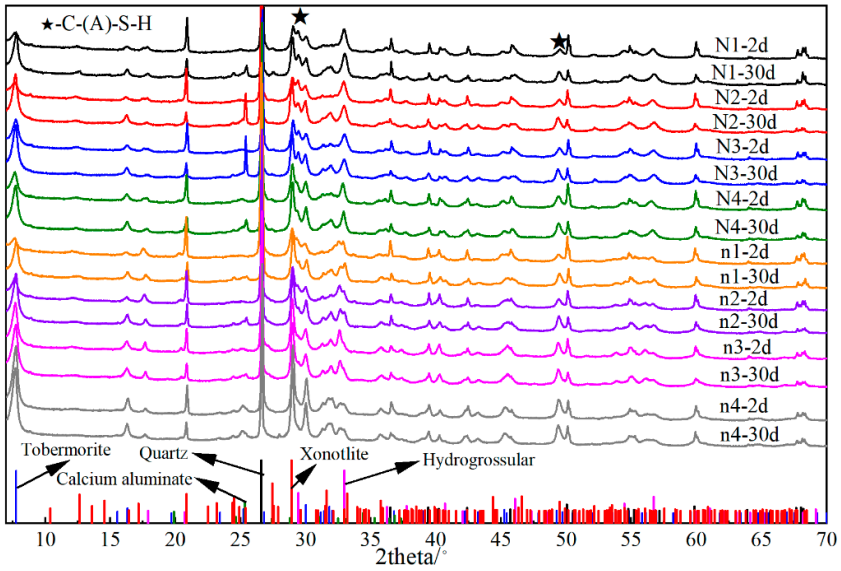


Figure 7. X-ray diffraction results of set cement during 2 d–30 d of curing (N1–N4: set and cured at 200 °C; n1–n4: set at 80 °C for 1 d and then cured at 200 °C).

To further clarify the evolution of mineral composition in the set cement under different curing regimes, quantitative phase analysis was performed using the Rietveld–PONKCS method along with the external standard method, as described in Section 2.3.4. The refinement results are summarized in Figure 8. As shown in the figure, the content of C-(A)-S-H in systems with different densities remained stable or increased slightly from 2 d to 30 d. Tobermorite content increased significantly, whereas xonotlite content remained low and stable. This phase evolution represents the main mechanism by which the cement systems resisted high-temperature strength retrogression. Compared with the high-temperature setting systems, the low-temperature setting systems contained more tobermorite and

less hydrogrossular and xonotlite. In addition, when the density decreased from 1.90 to 1.60 g/cm^3, the low-temperature setting systems retained more C-(A)-S-H than the corresponding high-temperature setting systems. These differences in mineral composition explain the superior macroscopic performance of the low-temperature setting systems at the same density.

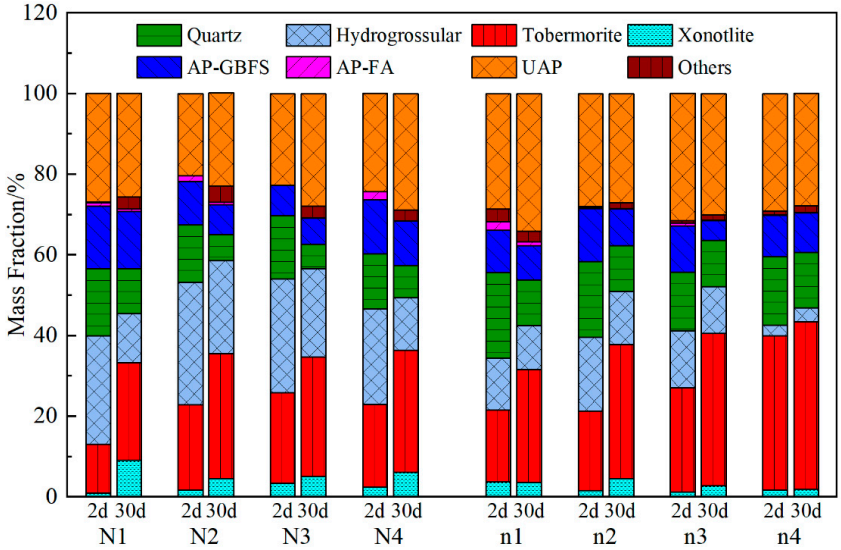


Figure 8. Phase composition evolution of set cement during 2 d–30 d of curing (N1–N4: set and cured at 200 °C; n1–n4: set at 80 °C for 1 d and then cured at 200 °C). Note: AP-GBFS represents amorphous phase of GBFS; AP-FA represents amorphous phase of fly ash; and UAP mainly refers to the unidentified amorphous phase, which is primarily composed of C-(A)-S-H gel.

Although the low-density systems prepared by water addition exhibited poor macroscopic properties, water addition had little effect on the C-(A)-S-H content. This indicates that the inferior performance was mainly caused by coarsening of the pore structure rather than changes in hydration products. When water was added to reduce slurry density, the solid-phase volume fraction decreased, water content increased, and initial porosity rose sharply (see Table 3), which hindered microstructural development and weakened macroscopic properties. Nevertheless, regardless of setting temperature, reducing density from 1.90 to 1.60 g/cm^3 by water addition slightly increased the total amount of hydration products, including both crystalline and amorphous phases. This suggests that the additional water promoted hydration. Specifically, when density decreased from 1.90 to 1.75 g/cm^3, the main change was an increase in the combined content of hydrogrossular and tobermorite. When density further decreased from 1.75 to 1.60 g/cm^3, the increase in total hydration products was mainly reflected by a slight increase in C-(A)-S-H content. After 30 d of curing, the systems containing hollow glass microspheres (N4 and n4) contained fewer crystalline products than the water-addition systems of the same density (N3 and n3), while maintaining comparable C-(A)-S-H contents. The low degree of crystallinity is beneficial for stabilizing cement strength. In summary, C-(A)-S-H, which plays a key role in strength development, remained stable in cement systems with different densities under both high- and low-temperature setting conditions.

3.5. Compositional Evolution of Cement Systems

Figure 9 shows the overall compositional evolution of cement systems by considering the mass of free water and chemical additives. For the systems whose density was reduced by water addition (N1–N3 and n1–n3), free water content increased with decreasing density, whereas for the systems whose density was reduced by the addition of hollow glass

microspheres (N4 and n4), the free water contents were comparable to those of N1 and n1. No crystalline phases originating from cement, slag, or fly ash were detected under these high-temperature conditions, indicating that these phases had reacted completely; therefore, the degrees of reaction of fly ash and GBFS were quantified by the reaction of the corresponding amorphous phases. Among the three mineral admixtures, fly ash exhibited the highest degree of reaction (84–100%) after 30 d of curing, which may be partially due to its lower addition level. The overall degree of reaction of GBFS (43–80%) was comparable to that of silica (46–76%) but varied widely. The degree of reaction of silica sand was lower in the low-temperature setting systems (46–56%) than in the high-temperature setting systems (57–76%). In contrast, the degree of reaction of GBFS was much higher in the low-temperature setting system (60–80%) compared to that in the high-temperature setting system (43–73%), and the difference is especially strong for the high-density slurries (n1 at 66% and N1 at 43%). The degrees of reaction of both silica sand and GBFS were the highest in slurries N3 and n3, suggesting that an increasing water-to-cement ratio increased reactivity. The addition of hollow glass microspheres appears to promote the reactivity of silica, as slurries N4 and n4 exhibited the most significant reduction in unreacted silica from 2 d to 30 d of curing.

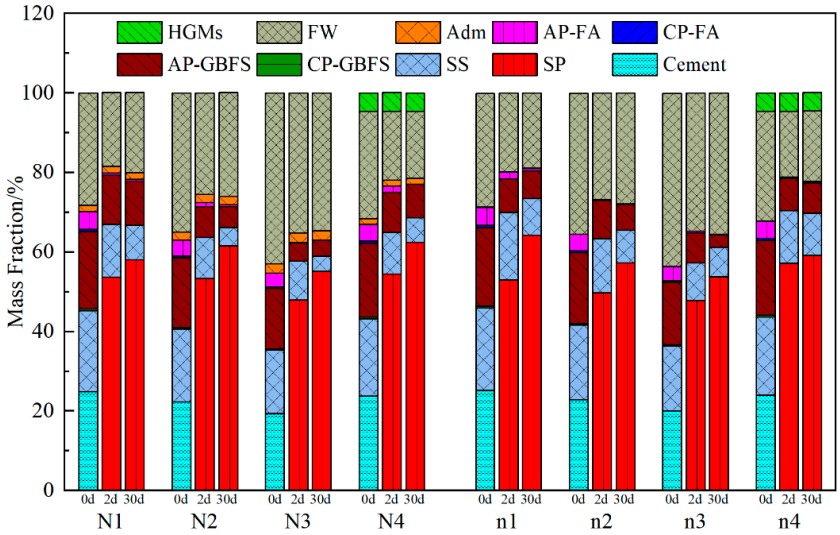


Figure 9. Composition evolution of set cement during 30 d of curing (N1–N4: set and cured at 200 °C; n1–n4: set at 80 °C for 1 d and then cured at 200 °C). Note: HGM: Hollow Glass Microspheres; FW: Free Water; Adm: Admixtures; AP-FA: Amorphous Phase of Fly Ash; CP-FA: Crystalline Phase of Fly Ash; AP-GBFS: Amorphous Phase of GBFS; CP-GBFS: Crystalline Phase of GBFS; SS: Silica Sand; HP: Hydration Products.

3.6. Thermogravimetry Analysis (TGA)

Figures 10 and 11 summarize the thermogravimetry (TG) results of the high-temperature setting systems and low-temperature setting systems, respectively. The derivative thermogravimetry (DTG) curves reveal distinct decomposition ranges and primary decomposition peaks corresponding to dehydration or thermal decomposition of specific hydrated phases. First, decomposition peaks near 200 °C remained stable or increased with curing time, and these peaks are typically associated with the dehydration of semi-crystalline C-S-H. Second, peaks near 400 °C generally exhibited decreasing trends and are mainly related to hydrogrossular decomposition. Third, all systems exhibited broad decomposition peaks within the range of 350–800 °C, which may involve the decomposition of multiple mineral phases, including tobermorite, hydrogrossular, and xonotlite. The peak near 760 °C may be related to xonotlite decomposition, while the peak around 850 °C may correspond to the decomposition of trace amounts of calcium aluminate phases.

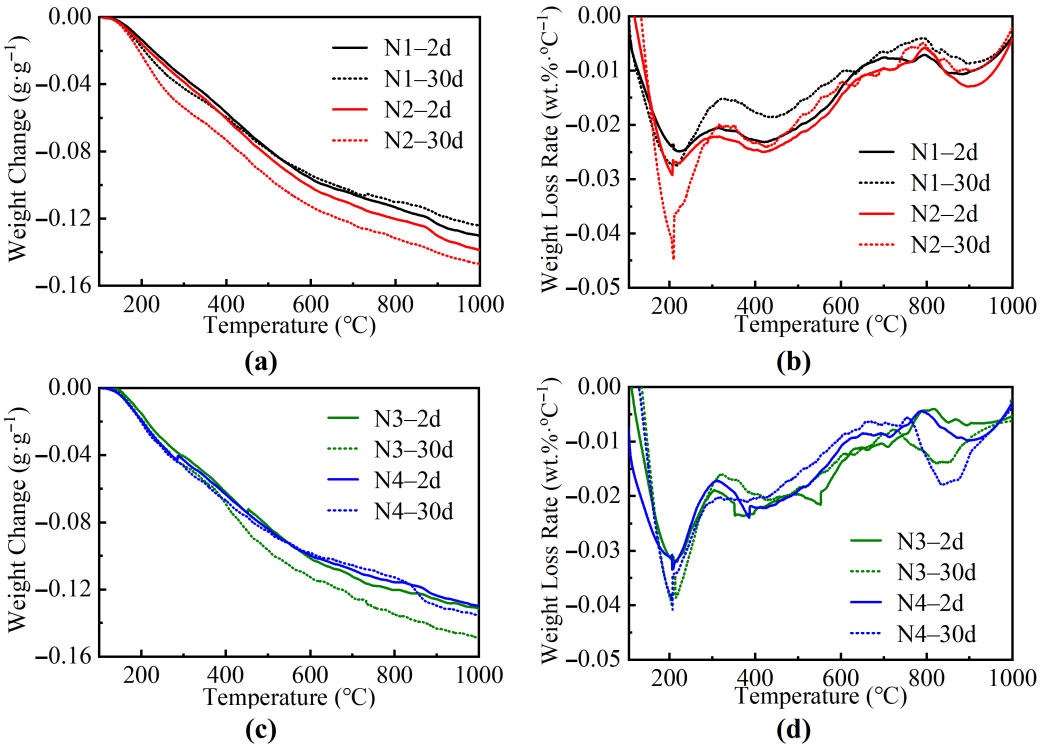


Figure 10. TGA results of high-temperature setting slurries: (**a**) TG curves of N1 and N2 systems; (**b**) DTG curves of N1 and N2; (**c**) TG curves of N3 and N4 systems; (**d**) DTG curves of N3 and N4.

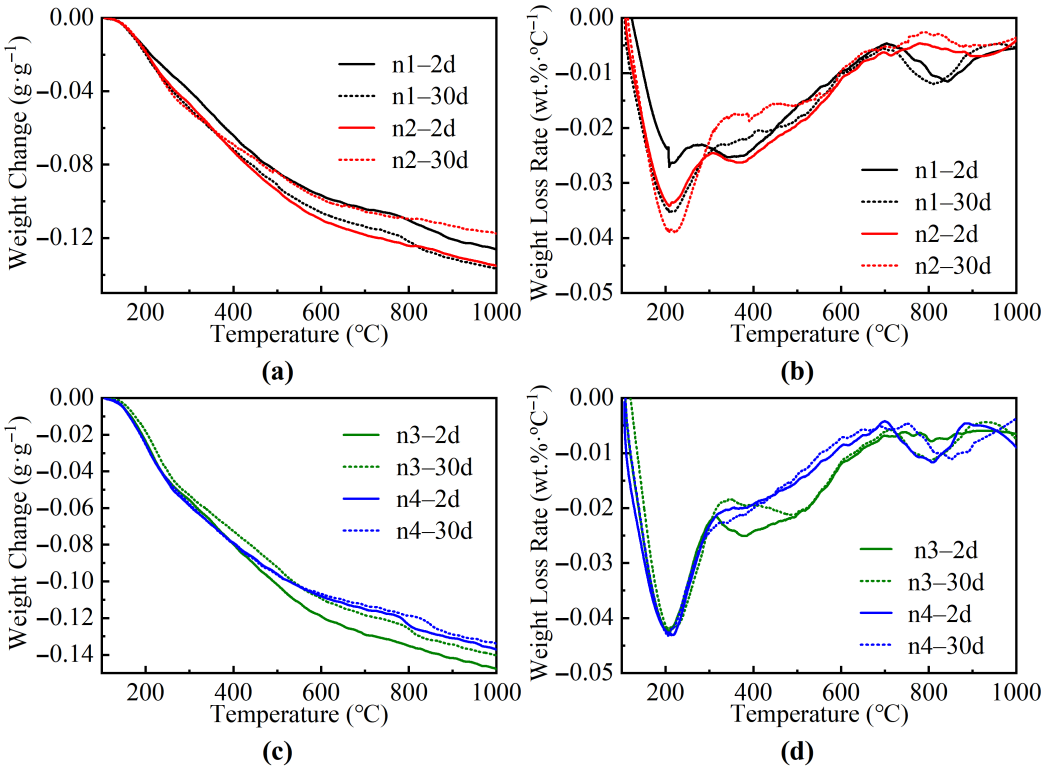


Figure 11. TGA results of low-temperature setting slurries: (**a**) TG curves of n1 and n2 systems; (**b**) DTG curves of n1 and n2; (**c**) TG curves of n3 and n4 systems; (**d**) DTG curves of n3 and n4 systems.

The TG curves mainly reflect the total bound water contents of the hardened cement. It can be observed that the bound water contents of N1 and N4 remained stable with

curing time, whereas those of N2 and N3 increased slightly, possibly because a higher water-to-cement ratio promoted further hydration of the mineral admixtures during the curing period from 2 d to 30 d. For the low-temperature setting systems, the bound water content in n1 increased slightly with curing time, while it decreased slightly with curing time in n2 and n3; slurry n4 exhibited almost no change in total bound water content. Overall, the total bound water content ranged from 0.11 to 0.15 g/g of dry cement, with only small variations among different systems. These test results further confirmed that the composition and microscopic structure of the hydrated well cement systems remained highly stable, regardless of the different curing regimes and slurry densities.

3.7. Correlations Between Macroscopic and Microscopic Properties of Set Cement

The above analyses in Sections 3.1–3.6 reported the compressive strength, water permeability, pore structure, phase composition, compositional evolution and thermal decomposition behavior of the retrogression-resistant cement systems with different densities and setting temperatures. Taken together, these results allow the relationships among slurry density, setting temperature, microstructure and macroscopic performance to be summarized as follows:

(1) The influence of density is mainly reflected in the pore structure. As the density decreased from 1.90 to 1.60 g/cm^3, both the total porosity and the proportion of pores larger than 50 nm increased, the compressive strength decreased, and the water permeability increased. The C-(A)-S-H content remained stable or increased slightly over 30 d of curing in all systems, indicating that the differences in macroscopic performance among systems of different densities mainly originate from the pore structure rather than from changes in the hydration products. When the density was reduced by incorporating hollow glass microspheres instead of additional water, both the total porosity and the proportion of pores larger than 50 nm were lower than those of the water-extended system of the same density, resulting in higher strength and lower permeability.

(2) The influence of setting temperature is reflected in both the pore structure and the phase composition. At the same density, systems set at 80 °C and subsequently cured at 200 °C exhibited higher 30 d compressive strength, lower water permeability, a smaller proportion of pores larger than 50 nm, higher tobermorite content, lower xonotlite and hydrogrossular contents, and more stable C-(A)-S-H. The differences in macroscopic performance between the two setting regimes are consistent with the differences in both pore structure and phase composition.

Overall, density affects macroscopic performance mainly through pore structure, whereas setting temperature affects macroscopic performance through both pore structure and phase assemblage. These two factors should therefore be considered together in the design of retrogression-resistant cement systems for deep and ultra-deep wells.

4. Conclusions

Retrogression-resistant oil well cement systems with different densities and prepared using Portland cement, silica sand, fly ash and ground blast furnace slag (GBFS) were designed to investigate the effects of setting temperature on their high-temperature performance at 2 d and 30 d. The main conclusions are as follows:

(1) Macroscopic property tests indicate that the compressive strength of the high-temperature setting systems remained stable during curing, whereas that of the low-temperature setting systems not only remained stable but also increased with curing time. Reducing slurry density by water addition significantly decreased compressive strength, while density reduction using hollow glass microspheres had a

much smaller adverse effect. Water permeability also remained relatively stable during the same curing period. For low-density systems, the water permeability of the low-temperature setting systems was significantly lower than that of the high-temperature setting systems, indicating that low-temperature setting was more beneficial for microstructural stability.

(2) Microstructural analysis indicates that the pore structure of the retrogression-resistant systems remained stable throughout the 30 d curing period, consistent with the macroscopic property test results. When slurry density was reduced by water addition, the proportion of harmful pores larger than 50 nm increased significantly, resulting in weaker low-density set cement. In contrast, reducing density by incorporating hollow glass microspheres produced a more favorable pore structure. Compared with the high-temperature setting systems, the low-temperature setting systems showed a significantly lower total proportion of harmful pores larger than 50 nm, which explains their superior macroscopic performance.

(3) Phase composition analysis indicates that the content of amorphous hydration products represented by C-(A)-S-H remained stable from 2 d to 30 d of curing in all systems; tobermorite content increased significantly, whereas xonotlite content remained low and relatively stable. Such phase evolution is the primary mechanism responsible for the retrogression-resistant behavior of the investigated systems. In addition, the low-temperature setting systems generally contained higher amounts of C-(A)-S-H and tobermorite and lower amounts of hydrogrossular and xonotlite than the high-temperature setting systems. These differences explain the superior performance of the low-temperature setting systems.

(4) Hydration extent analysis of different mineral admixtures shows that fly ash exhibited much higher reaction competitiveness than slag and silica. In the low-temperature setting systems, the degree of reaction of silica sand was lower, whereas the degree of reaction of GBFS was much higher than that in the high-temperature setting systems. These observations indicate that the reaction mechanisms of different mineral admixtures in retrogression-resistant oil well cement systems are highly complex and deserve further investigation.

Author Contributions: Conceptualization, X.P.; Methodology, G.C., J.Q. and X.P.; Validation, G.C. and J.D.; Formal analysis, J.Y., G.C. and Z.L.; Investigation, J.Y., G.C. and J.Q.; Resources, X.P., K.L. and J.S.; Data curation, J.Y., G.C. and Z.L.; Writing—original draft, J.Y., Z.L. and X.P.; Writing—review & editing, J.Y., G.C., J.Q., X.P. and J.D.; Visualization, J.Y. and G.C.; Supervision, X.P., K.L. and J.S.; Project administration, X.P.; Funding acquisition, X.P. and J.S. All authors have read and agreed to the published version of the manuscript.

Funding: This research received no external funding.

Data Availability Statement: The raw data supporting the conclusions of this article will be made available by the authors on request.

Acknowledgments: This research was funded by National Natural Science Foundation of China (Grant No. 52288101) and the Fund of State Key Laboratory of Deep Oil and Gas, China University of Petroleum (East China) (Grant No. SKLDOG2024-ZYTS-11).

Conflicts of Interest: Author Guodong Cheng was employed by the company SINOPEC Research Institute of Petroleum Engineering Co., Ltd. and Jiankun Qin was employed by the company Petroleum Engineering Technology Research Institute of Shengli Oilfield. The remaining authors declare that the research was conducted in the absence of any commercial or financial relationships that could be construed as a potential conflict of interest.

References

1. Krakowiak, K.; Thomas, J.; Musso, S.; James, S.; Akono, A.; Ulm, F. Nano-chemo-mechanical signature of conventional oil-well cement systems: Effects of elevated temperature and curing time. *Cem. Concr. Res.* **2015**, *67*, 103–121. [CrossRef]
2. Adefemi, A.; Sofoluwe, O.; Ekemezie, I.; Babayeju, O. Exploring technological and operational challenges in high-pressure: High-temperature drilling techniques. *Glob. J. Eng. Technol. Adv.* **2024**, *19*, 37–49. [CrossRef]
3. Pang, X.; Qin, J.; Sun, L.; Zhang, G.; Wang, H. Long-term strength retrogression of silica-enriched oil well cement: A comprehensive multi-approach analysis. *Cem. Concr. Res.* **2021**, *144*, 106424. [CrossRef]
4. Wang, C.; Feng, Q.; Liu, J.; Tang, H.; Yue, W.; Song, T. Adsorption of fluid loss additive and its interaction with retarder for well cementing: A fluorescence labeling investigation. *Colloids Surf. A Physicochem. Eng. Asp.* **2026**, *741*, 140227. [CrossRef]
5. Guo, J.; Chen, R.; Zheng, Y.; Zhang, H.; Hu, M. Research progress on high-temperature retarders for ultra-deep well cementing and prospects of intelligent efficiency enhancement technologies. *Nat. Gas. Ind.* **2025**, *45*, 152–167.
6. Liu, H.; Li, T.; Zhang, J.; Xu, P.; Xia, X.; Yu, Y.; Liu, L.; Chen, H. Thermodynamic mechanism of silica dosage and temperature on phase composition of well cement at high temperature and its impact on macro-properties. *Appl. Geochem.* **2025**, *180*, 106294. [CrossRef]
7. Pernites, R.; Santra, A. Portland cement solutions for ultra-high temperature wellbore applications. *Cem. Concr. Compos.* **2016**, *72*, 89–103. [CrossRef]
8. Krakowiak, K.; Thomas, J.; James, S.; Abuhaikal, M.; Ulm, F. Development of silica-enriched cement-based materials with improved aging resistance for application in high-temperature environments. *Cem. Concr. Res.* **2018**, *105*, 91–110. [CrossRef]
9. de Sena Costa, B.; de Souza, G.; de Oliveira Freitas, J.; da Silva Araujo, R.; Santos, P. Silica content influence on cement compressive strength in wells subjected to steam injection. *J. Pet. Sci. Eng.* **2017**, *158*, 626–633. [CrossRef]
10. Makar, J.; Luke, K. Impact of Steam Treatment on the Microstructure and Chemistry of Cured Oil Well Cements. In Proceedings of the 13th International Congress on the Chemistry of Cement, Madrid, Spain, 3–8 July 2011.
11. Ma, F.T.; Wen, Y.K.; Yang, Y.Y.; Zeng, D.C.; Hu, W.T.; Sang, Y.; Huang, H.L.; Wei, J.X.; Yu, Q.J. Early strength retrogression of silica-rich oil well cement under 200 °C hydrothermal conditions: Structural degradation associated with progressive expansion. *Pet. Sci.* **2026**. [CrossRef]
12. Alavoine, A.; Lecomte, M.; Saillio, M.; Duc, M.; Ghabezloo, S. Effect of the hydration temperature between 110 and 190 °C on the microstructure of Class G cement: Phase composition, pore structure and C–S–H chemistry. *Cem. Concr. Res.* **2026**, *200*, 108093. [CrossRef]
13. Zhao, F.; Wang, C.; Yang, T.; Wang, H. Mechanics and Phase–Microstructure Evolution of Silica Sand-Modified Oil-Well Cement Cured at 240 °C: From Single-Size Effects to Graded-Packing Design. *J. Compos. Sci.* **2026**, *10*, 103. [CrossRef]
14. Cheng, G.; Li, H.; Liu, H.; Wei, H.; Zhou, S.; Fang, K. Strength retrogression mechanisms of silica-enriched oil well cement under 240 °C curing conditions. *Chem. Pap.* **2026**, *80*, 1653–1663. [CrossRef]
15. Yu, Y.; Guo, C.; Liu, H.; Li, M.; Liu, L. Microstructure optimization and strength enhancement of oil well cement at 240 °C via γ-alumina nanoparticle-induced hydration control. *J. Dispers. Sci. Technol.* **2026**, 1–12. [CrossRef]
16. Paiva, M.; Silva, E.; Melo, D.; Martinelli, A.; Schneider, J. A geopolymer cementing system for oil wells subject to steam injection. *J. Pet. Sci. Eng.* **2018**, *169*, 748–759. [CrossRef]
17. Fu, C.; Wang, H.; Zhan, H.; Li, Y.; Li, S.; Yin, B. Reactivity-Controlled Dual Silicon Sources Drive CSH Crystallization and Property Enhancement at Low Ca/Si Ratios. *Mater. Today Commun.* **2025**, *49*, 114161. [CrossRef]
18. Reddy, B.; Zhang, J.; Ellis, M. Cement strength retrogression issues in offshore deep water applications-do we know enough for safe cementing? In Proceedings of the Offshore Technology Conference, Houston, TX, USA, 2–5 May 2016; p. D011S002R004.
19. Cheng, G.; Pang, X.; Wang, H.; Sun, J.; Qiu, Z. Anti-strength retrogression cementing materials for deep and ultra-deep wells. *Constr. Build. Mater.* **2024**, *411*, 134407. [CrossRef]
20. Chow, S.; Kalousek, G. Research on cements for geothermal and deep oil wells. *Soc. Pet. Eng. J.* **1976**, *16*, 307–309. [CrossRef]
21. Shaw, S.; Clark, S.; Henderson, C. Hydrothermal formation of the calcium silicate hydrates, tobermorite ($Ca_5Si_6O_{16}(OH)_2{\cdot}4H_2O$) and xonotlite ($Ca_6Si_6O_{17}(OH)_2$): An in situ synchrotron study. *Chem. Geol.* **2000**, *167*, 129–140. [CrossRef]
22. Zheng, S.; Gu, H.; Liu, T.; Dai, T.; Jiang, G.; Xu, H.; Lai, H.; Chen, M.; Wan, T. Effect of rice husk ash on the compressive strength and microstructural characteristics of low-density cement slurry under different temperature conditions. *Geoenergy Sci. Eng.* **2025**, *257*, 214178. [CrossRef]
23. Wang, Y. Research and Application of Solid Composite Microsphere Low-Density Cement Slurry System. *J. Phys. Conf. Ser.* **2025**, *3048*, 012052. [CrossRef]
24. Yue, J.; Liu, Z.; Wang, J.; Sun, T.; Wu, Z.; Geng, Y. A Low-Cost and Low-Density Cement Slurry System Suitable for a Shallow Unconsolidated Stratum. *Adv. Mater. Sci. Eng.* **2020**, *2020*, 1628281. [CrossRef]
25. Song, L.; Wang, C.; Liu, J.; Li, D. Temperature-responsive micro-cross-linking: A novel solution for enhancing high-temperature viscosity and settlement stability of high-density cement slurry. *Gels* **2025**, *11*, 138. [CrossRef] [PubMed]

26. Abdelaal, A.; Elkatatny, S.; Abdel Fattah, A. Perlite incorporation for sedimentation reduction and improved properties of high-density geopolymer cement for oil well cementing. *Sci. Rep.* **2024**, *14*, 9707. [CrossRef] [PubMed]
27. Wei, J.; Li, L. Research of optimization design of high-performance high-density cement slurry system with close packing technology. *AIP Conf. Proc.* **2019**, *2073*, 020002. [CrossRef]
28. Kalyoncu, R.S.; Snyder, M.J. *High-Temperature Cementing Materials for Completion of Geothermal Wells*; Final Report; Battelle Columbus Laboratories: Columbus, OH, USA, 1981.
29. Wang, H.; Ma, C.; Yuan, Y.; Chen, Y.; Liu, T.; An, C.; Wang, N. Lightweight insulating oil-well cement filled with hollow glass microspheres and numerical simulation of its unsteady heat transfer process. *Adv. Compos. Hybrid. Mater.* **2024**, *7*, 98. [CrossRef]
30. Mutua, F.; Lin, P.; Koech, J.; Wang, Y. Surface Modification of Hollow Glass Microspheres. *Mater. Sci. Appl.* **2012**, *3*, 856–860.
31. Cheng, G.; Pang, X.; Qiu, Z.; Qin, J.; Li, N. Well cement composition optimization for deep well applications. In Proceedings of the ISRM Congress, Salzburg, Austria, 9–14 October 2023.

Disclaimer/Publisher's Note: The statements, opinions and data contained in all publications are solely those of the individual author(s) and contributor(s) and not of MDPI and/or the editor(s). MDPI and/or the editor(s) disclaim responsibility for any injury to people or property resulting from any ideas, methods, instructions or products referred to in the content.